Journal of Sound and Vibration 330 (2011) 652–663

Contents lists available at ScienceDirect

Journal of Sound and Vibration

journal homepage: www.elsevier.com/locate/jsvi

Effects of local surface residual stresses on the near resonance vibrations of nano-beams

B. Bar On *, E. Altus

Faculty of Mechanical Engineering, Technion – Israel Institute of Technology, 32000 Haifa, Israel

ARTICLE INFO

Article history:
Received 13 May 2010
Received in revised form
24 August 2010
Accepted 25 August 2010
Handling Editor: S. Ilanko
Available online 21 September 2010

ABSTRACT

The effects of surface residual stresses on nano-beams including mid-plane stretching under near resonance vibrations, are studied. The nonlinear vibration equations are separated into two complementary parts: static, which includes the surface residual moments and yields a residual deflection, and dynamic, for the beam vibrations associated with the residual deflection via geometrical nonlinearity. The dynamic response is expressed by a shape mode expansion with time dependent coefficients, governed by a set of coupled ordinary differential equations. An approximated solution is extracted analytically by a combination of the asymptotic straight-forward expansion and multiple scale method. Results exhibit fine correspondence with finite element simulations. It is found that the non-uniformities in the surface residual stresses change the resonance frequency of the beam, shifts its amplitude-response curve and reduce its phase. Applications for nano-sensors are demonstrated and optimization possibilities are discussed.

1. Introduction

Residual stresses and modulus are noticeable mechanical properties in the micro–nano scales. The latter, however, can be neglected for sufficiently thick elements [1]. A mechanical modeling of structures including surface effects was initiated by Gurtin and Murdoch [2], who proposed the kinematic and constitutive relations for a bulk coated by an infinitesimal thick surface layer. Their work was followed by a variety of studies on structures under both static and dynamic loadings. In 2004, Lim and He [3] analyzed thin plates including surface residual stresses and modulus effects with geometric nonlinearity (Von Karman's strains). They formulated and solved the equations for several cases of infinitely broad hinged plates under static bending, buckling and free vibrations. The significance of the surface effects was observed for a length scale below 10^{-8} m. In 2006, Lu et al. [4] proposed a mechanical model for surface effects in plates. Their work proposed the dynamic governing equations for both Kirchhoff and Mindlin plate theories. Two case studies of static bending and free vibrations in infinitely broad hinged plates were solved and size effects of the mechanical features due to surface properties were provided. In both works of Lim and He [3] and Lu et al. [4], no validation was given by either simulations or experiments. In 2010, Sheng et al. [5] studied the surface effects on the free vibrations of MEMS, by considering a laminated plate theory for the bulk and surface layers. Recently, Bar On et al. [6] proposed a static mechanical model for non-uniform surface effects in nano-beams. By allowing longitudinal and transverse surface heterogeneity, they concluded that the surface effects yield longitudinal stiffness heterogeneity of the beam cross-section, accompanied by surface distributed

* Corresponding author.
E-mail addresses: benny.bar-on@weizmann.ac.il, benny@tx.technion.ac.il, bbarontx@weizmann.ac.il (B. Bar On).

0022-460X/$ - see front matter © 2010 Elsevier Ltd. All rights reserved.
doi:10.1016/j.jsv.2010.08.033

residual forces and moments. Their model, which based on Euler–Bernoulli assumptions for laminated beams [7], was validated by atomistic simulations of beam like structures with non-uniform surface configuration.

Surface effects on the resonance frequency of beams, were studied experimentally by Lu et al. [8] on a double coated, 1 μm thin, cantilever. Variations of 1 percent which observed in the resonance frequency, were attributed to the surface modulus. In 2006, Tamayo et al. [9] studied the effect of adsorption-induced local non-uniformity on the resonance frequency of a cantilever. Their analysis was based on the assumption that the non-uniformity has a negligible effect on the shape of the normal modes. In agreement with Lu et al. [4], Tamayo et al. [9] observed a ± 0.5 percent changes of the resonance frequency. In 2008, Zhang et al. [10] studied the effects of adsorption induced surface modulus on the resonance frequency of nano-scale beams using atomistic simulations. They reported that these effects are noticeable (about 3 percent variations) for beams with thickness of 20 nm or less. The relatively small variations are attributed to the weak effect of the surface modulus, while the stronger effects of surface residual stresses were absent in cantilever vibrations [11,12].

Surface effects are commonly used in small scale adsorption induced sensing mechanisms [13]. A variety of methods were developed for using small scale beams for the adsorption detection of chemical and biological elements [14–16]. Recently, Bar On and Altus [17] analyzed the effects of local stochastic adsorption-induced surface residual stresses on the mechanical responses of nano-beams. Cherian and Thundat [18] demonstrated the detectability of sodium (Na) adsorption on a silicon nitride cantilever by its resonance shift and reported a greater resonance shift for higher concentration of sodium. To the best of our knowledge, previous studies of vibrating nano-beam sensors have not considered the effects of non-uniform surface residual stresses.

In this work we propose a mechanical model for flexural vibrations in nano-beams including surface heterogeneity and nonlinear mid-plane stretching effects. The current work generalizes previous quasi-static heterogeneous models [6,17] by considering external periodic excitations. Since the surface heterogeneity effects are significant near the first resonance frequencies (Section 5), the scope is on low wavenumbers in which the transverse shear, longitudinal and rotary inertial effects can be neglected. The analysis is conducted for sufficiently thick elements in which surface modulus effects are negligible. By considering both surface heterogeneity and mechanical nonlinearity, the effect of surface residual stresses leads to considerable variations in the dynamic amplitude-response curve.

2. Mechanical model

Consider a slender beam with length L, height h and breadth b, associated with the in-plane coordinate system $(\hat{x},\hat{y})$ and center-line displacements $(\hat{u},\hat{w})$, as shown in Fig. 1. Restricting the analysis to flexural vibrations with long wavelengths compared to the radius of gyration, Euler–Bernoulli assumptions can be adopted and the beam displacement field $(\tilde{u},\tilde{w})$ can be approximated by the center-line displacements $(\hat{u},\hat{w})$ through

$$\tilde{u} = \hat{u} - \hat{y}\frac{d\hat{w}}{d\hat{x}} \tag{1}$$

$$\tilde{w} = \hat{w} \tag{2}$$

Introducing Von Karman's axial strain, the strain-displacements relation is

$$\varepsilon = \frac{d\hat{u}}{d\hat{x}} - \hat{y}\frac{d^2\hat{w}}{d\hat{x}^2} + \frac{1}{2}\left(\frac{d\hat{w}}{d\hat{x}}\right)^2 \tag{3}$$

In small scale beams, the cross-section is associated with three normal stress components: bulk stress σ^0 and two singular surface stresses, σ^+ and σ^- along the upper and lower surfaces, respectively. Considering linear elastic material, σ^0 refers

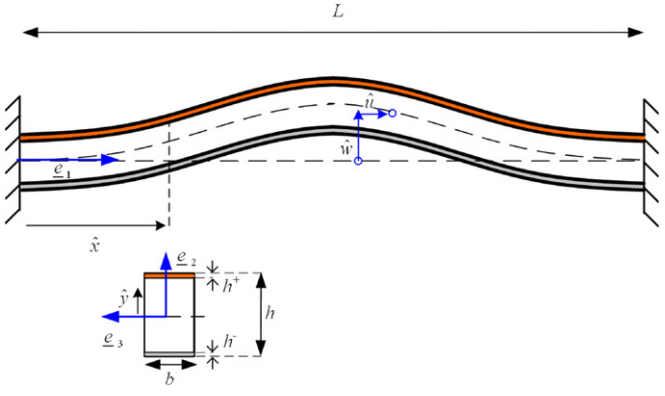

Fig. 1. Schematic description of 1D nano-beam and its center-line displacements. The structure is composed of three layers, uniform bulk layer coated by two non-uniform surface layers.

to ε through Young's modulus E. By assuming sufficiently thick beam [1], σ^+ and σ^- include only the effects of surface residual stresses, τ^+ and τ^-:

$$\sigma^0 = E\varepsilon, \quad \sigma^+ = -\tau^+\delta\left(\hat{y}-\frac{h}{2}\right), \quad \sigma^- = -\tau^-\delta\left(\hat{y}+\frac{h}{2}\right) \tag{4}$$

Without lose of generality, positive values for τ^+ and τ^- corresponds to compressive residual stresses. Neglecting the longitudinal and rotary inertial effects, force and moment equilibrium on a nano-beam segment (Fig. 2), associated with first-order Taylor approximation, yields

$$\sum F_{e_1} = \frac{d}{d\hat{x}}\hat{F}_1(\hat{x}) = \frac{d}{d\hat{x}}\left[\int_0 \sigma^0 b\, d\hat{y} + \int_+ \sigma^+ b\, d\hat{y} + \int_- \sigma^- b\, d\hat{y}\right] = 0 \tag{5}$$

$$\sum F_{e_2} = \frac{d}{d\hat{x}}\hat{F}_2 - \hat{\mu}\frac{d\hat{w}}{d\hat{t}} + \hat{\Gamma}_2 = \rho A\frac{d^2\hat{w}}{d\hat{t}^2} \tag{6}$$

$$\sum M = \frac{d}{d\hat{x}}\hat{M}(\hat{x}) + \hat{F}_2(\hat{x}) = -\frac{d}{d\hat{x}}\left[\int_0 \sigma^0 b\hat{y}\, d\hat{y} + \int_+ \sigma^+ b\hat{y}\, d\hat{y} + \int_- \sigma^- b\hat{y}\, d\hat{y}\right] - \frac{d\hat{w}}{d\hat{x}}\left[\int_0 \sigma^0 b\, d\hat{y} + \int_+ \sigma^+ b\, d\hat{y} + \int_- \sigma^- b\, d\hat{y}\right] + \hat{F}_2(\hat{x}) = 0 \tag{7}$$

$\hat{F}_1, \hat{F}_2$ and $\hat{M}$ denote the resultant cross-sectional forces and moment, respectively, ρ is the specific mass, $A=bh$ is the cross-sectional area, $\hat{\mu}$ is Coulomb's friction coefficient and $\hat{\Gamma}_2$ is an external distributed force parallel to $\underline{e}_2$. Coulomb's friction model is adopted to provide a simplified approximation for the dissipation effects.

Introducing the non-dimensional parameters

$$x = \frac{\hat{x}}{L}, \quad u = \frac{\hat{u}}{L}, \quad w = \frac{\hat{w}}{L}, \quad \hat{t} = t\sqrt{12\frac{\rho}{E}\frac{L^4}{h^2}} \tag{8}$$

Substituting (1)–(4) into (5)–(7), deriving (7) and substitute it into (6) and using (8), yields (after some algebra)

$$\frac{d}{dx}\left[f_s - a\left(\frac{\partial u}{\partial x} + \frac{1}{2}\left(\frac{\partial w}{\partial x}\right)^2\right)\right] = 0 \tag{9}$$

$$\frac{\partial^4 w}{\partial x^4} + \frac{\partial}{\partial x}\left\{\frac{\partial w}{\partial x}\left[f_s - a\left(\frac{\partial u}{\partial x} + \frac{1}{2}\left(\frac{\partial w}{\partial x}\right)^2\right)\right]\right\} + \frac{\partial^2 w}{\partial t^2} + \mu\frac{\partial w}{\partial t} = \frac{d^2 m_s}{dx^2} + \gamma_2 \tag{10}$$

where a, γ_2 and μ are the non-dimensional axial stiffness, distributed transverse load and friction coefficient, respectively,

$$a = 12\left(\frac{L}{h}\right)^2 \tag{11}$$

$$\gamma_2 = \Gamma_2 L \Big/ \left[E\frac{bh}{12}\left(\frac{h}{L}\right)^2\right] \tag{12}$$

$$\mu = \frac{\hat{\mu}L}{\sqrt{E\frac{hb}{12}\left(\frac{h}{L}\right)^2 \rho bh}} \tag{13}$$

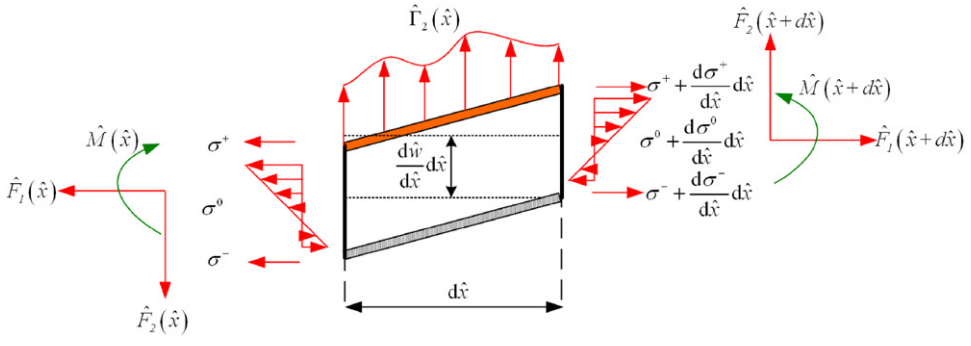

Fig. 2. Free body diagram on a nano-beam segment. $\hat{F}_1, \hat{F}_2$ and $\hat{M}$ are denoted for the resultant cross-sectional forces and moment, respectively, originated from the longitudinal stress field σ^0, σ^+ and σ^-.

Table 1
Comparison of the proposed model with previous nano-beams vibrations models.

	Lu	LH	Ta	Present
Surface heterogeneity	No	No	Yes	Yes
Nonlinear strains	No	Yes	No	Yes
Origin of surface effects	Modulus	Modulus	Modulus	Residual stresses

Lu ≡ Lu et al. [4], LH ≡ Lim and He [3], Ta ≡ Tamayo et al. [9]. The surface effects in the present model are attributed to the surface residual stresses, contrary to the weaker effect of surface modulus reported in previous studies.

$f_s(x)$, $m_s(x)$ are the non-dimensional, surface residual force and moment, respectively,

$$f_s(x) = 12\frac{1}{Eh}(\tau^+(x)+\tau^-(x))\left(\frac{L}{h}\right)^2 \tag{14}$$

$$m_s(x) = 6\frac{1}{Eh}(\tau^-(x)-\tau^+(x))\left(\frac{L}{h}\right) \tag{15}$$

Eqs. (9) and (10) are partial nonlinear coupled equations for governing the nano-beam vibrations, which generally do not have an analytical solution. These equations, however, can be simplified by integrating (9) and defining the total force (compressive) on the beam cross-section as

$$\lambda^2 = f_s - a\left(\frac{\partial u}{\partial x}+\frac{1}{2}\left(\frac{\partial w}{\partial x}\right)^2\right) \tag{16}$$

Letting $u_0 = u(x=0)$ and integrating (16) yields the following expression for the axial displacement field:

$$u(x)-u_0 = a^{-1}\left[\int_0^1 f_s(x)\,dx - \lambda^2 - \frac{1}{2}\int_0^1\left(\frac{dw}{dx}\right)^2 dx\right] \tag{17}$$

Following (16) and (17), λ^2 is determined according to the axial boundary conditions at x=1. Two conditions are admissible at x=1: fixed boundary force (γ_1), for which $\lambda^2 = -\gamma_1$ or displacements (u_1) for which λ^2 is found from (17). Positive γ_1 corresponds to tensile axial force. Summarizing the above

$$\lambda^2 = \begin{cases} -\gamma_1 & \text{Fixed force} \\ \int_0^1 f_s\,dx + a\left(u_0-u_1-\frac{1}{2}\int_0^1\left(\frac{\partial w}{\partial x}\right)^2\right)dx & \text{Fixed displacement} \end{cases} \tag{18}$$

Substituting (16) into (10), yields

$$\frac{\partial^4 w}{\partial x^4}+\lambda^2\frac{\partial^2 w}{\partial x^2}+\frac{\partial^2 w}{\partial t^2}+\mu\frac{\partial w}{\partial t} = \frac{d^2 m_s}{dx^2}+\gamma_2 \tag{19}$$

Complementary initial conditions, for $w(x,t=0)$ and $(dw/dt)(x,t=0)$ should be specified. The admissible boundary conditions for the deflection, slope, force and moment, respectively, and no other external loads, are

$$w=0, \quad \frac{\partial}{\partial x}w = m_s, \quad \frac{\partial^2}{\partial x^2}w = m_s, \quad \frac{\partial^3}{\partial x^3}w+\lambda^2\frac{\partial}{\partial x}w = \frac{\partial}{\partial x}m_s \tag{20}$$

By using the variable transformation above, the axial displacement (17) is decoupled from the nonlinear transverse vibration equations (18) and (19). Surface effects are exhibited by integration of the surface force ($\int_0^1 f_s\,dx$) and the surface distributed moment (d^2m_s/dx^2). The axial displacement is proportional to $\int_0^1 f_s\,dx$ (17). In axially determined beams, the vibration are governed by a linear partial differential equation. In axially indeterminate beams, however, $\lambda^2(w)$ and the resultant nonlinear equation are affected by the surface force and moment ($\int_0^1 f_s\,dx$ and m_s).

The current model generalizes and unifies several previous models. When surface heterogeneity is omitted, the present model reduce to Lim and He [3] and when nonlinearity is also omitted, it coincides with Lu et al. [4]. The configuration of Tamayo et al. [9] can be described by considering surface heterogeneity without nonlinear effects. In all of these cases, only the effect of surface modulus was relevant to the nano-beams vibrations. The comparison is summarized in Table 1. Note that in case of $\tau^+,\tau^- = 0$, (17)–(19) reduce to the common nonlinear vibrations equations [19].

3. Vibration equations for nano-beams with weak nonlinearity

Considering nano-beams with weak geometric nonlinearity (axially fixed edges u_1,u_0=0), let us denote $\varepsilon \approx h/L \ll 1$ as a non-dimensional scaling parameter. For typical nano-beams [20] subjected to weak excitations, weak dissipation and small displacements, the non-dimensional parameters in (17)–(20) are scaled by $\mu = \tilde{\mu}/\varepsilon$, $f_s = \tilde{f}_s$, $m_s = \varepsilon^2\tilde{m}_s$, $a = \tilde{a}/\varepsilon^3$, $\gamma_2 = \varepsilon^3\tilde{\gamma}_2$, $u = \varepsilon^2\tilde{u}$ and $w = \varepsilon^2\tilde{w}$, where $\tilde{f}_s,\tilde{m}_s,\tilde{a},\tilde{\mu},\tilde{\gamma}_2,\tilde{u}$, $\tilde{w} \in \mathcal{O}(1)$ [21]. Following the above, the deflection governing

equations for nano-beam are (tildes were dropped for compactness)

$$\frac{\partial^4 w}{\partial x^4}+\left(\int_0^1 f_s\,dx-\varepsilon a\int_0^1\frac{1}{2}\left(\frac{\partial w}{\partial x}\right)^2 dx\right)\frac{\partial^2 w}{\partial x^2}+\frac{\partial^2 w}{\partial t^2}+\varepsilon\mu\frac{\partial w}{\partial t}=\frac{d^2 m_s}{dx^2}+\varepsilon\gamma_2 \tag{21}$$

$$w=0,\quad \frac{d}{dx}w=0,\quad \frac{d^2}{dx^2}w=m_s,$$

$$\frac{\partial^3}{\partial x^3}w+\left(\int_0^1 f_s\,dx-\varepsilon a\int_0^1\frac{1}{2}\left(\frac{\partial w}{\partial x}\right)^2 dx\right)\frac{\partial}{\partial x}w=f_s \tag{22}$$

Let us express w as a superposition of two components, static and dynamic

$$w(x,t)=w_x(x)+w_{xt}(x,t) \tag{23}$$

where w_x is defined as the solution of

$$\frac{d^4 w_x}{dx^4}+\left(\int_0^1 f_s\,dx-\varepsilon a\int_0^1\frac{1}{2}\left(\frac{d}{dx}w_x\right)^2 dx\right)\frac{d^2 w_x}{dx^2}=\frac{d^2 m_s}{dx^2} \tag{24}$$

$$w_x=0,\quad \frac{d}{dx}w_x=0,\quad \frac{d^2}{dx^2}w_x=m_s$$

$$\frac{\partial^3}{\partial x^3}w_x+\left(\int_0^1 f_s\,dx-\varepsilon a\int_0^1\frac{1}{2}\left(\frac{\partial w_x}{\partial x}\right)^2 dx\right)\frac{\partial}{\partial x}w_x=\frac{\partial}{\partial x}m_s \tag{25}$$

Substituting (24) into (21) and (22) and eliminating terms according to (24) and (25), yields the following equation for w_{xt} and its corresponding boundary conditions:

$$\frac{\partial^4 w_{xt}}{\partial x^4}+\left(\int_0^1 f_s\,dx\right)\left(\frac{\partial^2 w_{xt}}{\partial x^2}\right)+\frac{\partial^2 w_{xt}}{\partial t^2}=\varepsilon\left\{\begin{array}{c}\gamma_2-\mu\dfrac{\partial w_{xt}}{\partial t}\\ +\left[a\dfrac{1}{2}\displaystyle\int_0^1\left(\frac{\partial w_{xt}}{\partial x}\right)^2 dx\right]\left(\dfrac{\partial^2 w_{xt}}{\partial x^2}\right)\\ +W(x,t)\end{array}\right\} \tag{26}$$

$$w_{xt}=0,\quad \frac{d}{dx}w_{xt}=0,\quad \frac{d^2}{dx^2}w_{xt}=0$$

$$\frac{\partial^3}{\partial x^3}w_{xt}+\left(\int_0^1 f_s\,dx\right)\frac{\partial}{\partial x}w_{xt}-\varepsilon a\frac{1}{2}\left[\int_0^1\left(\frac{\partial w}{\partial x}\right)^2 dx\frac{\partial w}{\partial x}-\int_0^1\left(\frac{\partial w_x}{\partial x}\right)^2 dx\frac{\partial w_x}{\partial x}\right]=0 \tag{27}$$

For brevity, (27d) is expressed by w and w_{xt} and W represents the coupling terms between w_x and w_{xt}:

$$W(x,t)=\left[a\frac{1}{2}\int_0^1\left(2\frac{\partial w_{xt}}{\partial x}\frac{dw_x}{dx}+\left(\frac{\partial w_x}{\partial x}\right)^2\right)dx\right]\left(\frac{\partial^2 w_{xt}}{\partial x^2}\right)+\left[a\frac{1}{2}\int_0^1\left(\left(\frac{\partial w_{xt}}{\partial x}\right)^2+2\frac{\partial w_{xt}}{\partial x}\frac{dw_x}{dx}\right)dx\right]\left(\frac{d^2 w_x}{dx^2}\right) \tag{28}$$

Note that the static surface induced deflection, which can be extracted independently of the dynamic response, affect w_{xt} via $W(x,t)$. The decoupled formulation in (23) can be further generalized for slowly varying adsorption-induced surface residual stresses, as commonly appear in small scale sensors [17].

Consider the following expansion for w_{xt}:

$$w_{xt}(x,t)=\sum_{m=1}^{\infty}\boldsymbol{\psi}_m(x)\boldsymbol{\varphi}_m(t) \tag{29}$$

where $\boldsymbol{\psi}_m(x)$ are the normal modes of the linear part in (26). Substituting (29) into (26)–(28), multiplying by $\boldsymbol{\psi}_n(x)$, integrating over x and using the orthogonal property, yields (after some algebra) the following differential equation for $\boldsymbol{\varphi}_m(t)$ of each mode:

$$\frac{\partial^2\boldsymbol{\varphi}_n(t)}{\partial t^2}+\sum_{m=1}^{\infty}\boldsymbol{\varphi}_m(t)\mathbf{K}_{mn}=\varepsilon\left\{\begin{array}{c}\mathbf{F}_n(t)-\mu\dfrac{\partial\boldsymbol{\varphi}_n(t)}{\partial t}\\ +a\dfrac{1}{2}\sum_{m,p,q=1}^{\infty}\boldsymbol{\varphi}_p(t)\boldsymbol{\varphi}_q(t)\boldsymbol{\varphi}_m(t)\boldsymbol{\Gamma}_{pq}\boldsymbol{\Upsilon}_{mn}\\ +\mathbf{W}_n(t)\end{array}\right\} \tag{30}$$

where $\mathbf{K}_{mn}$, $\mathbf{F}_n(t)$ and $\mathbf{W}_n(x,t)$ are the stiffness matrix, excitation and coupling vectors, respectively,

$$\mathbf{K}_{mn} = \boldsymbol{\varphi}_{mn} + \boldsymbol{\Upsilon}_{mn} \int_0^1 f_s \, dx \tag{31}$$

$$\mathbf{F}_n(t) = \int_0^1 \boldsymbol{\psi}_n(x) \gamma_2(x,t) \, dx \tag{32}$$

$$\mathbf{W}_n(t) = \int_0^1 \boldsymbol{\psi}_n(x) W(x,t) \, dx = a \sum_{m,p=1}^{\infty} \boldsymbol{\varphi}_p(t) \boldsymbol{\varphi}_m(t) \boldsymbol{\eta}_p \boldsymbol{\Upsilon}_{mn} + a \frac{1}{2} \int_0^1 \left(\frac{\partial w_x}{\partial x} \right)^2 dx \left(\sum_{m=1}^{\infty} \boldsymbol{\varphi}_m(t) \boldsymbol{\Upsilon}_{mn} \right) + a \frac{1}{2} \xi_n \sum_{p,q=1}^{\infty} \boldsymbol{\varphi}_p(t) \boldsymbol{\varphi}_q(t) \boldsymbol{\Gamma}_{pq} + a \xi_n \sum_{p=1}^{\infty} \boldsymbol{\varphi}_p(t) \boldsymbol{\eta}_p \tag{33}$$

$\boldsymbol{\varphi}_{mn}$, $\boldsymbol{\Gamma}_{pq}$, $\boldsymbol{\Upsilon}_{mn}$, $\boldsymbol{\eta}_p$ and ξ_n are the following projection relations:

$$\boldsymbol{\varphi}_{mn} = \int_0^1 \frac{d^4 \boldsymbol{\psi}_m}{dx^4} \boldsymbol{\psi}_n \, dx, \quad \boldsymbol{\Gamma}_{pq} = \int_0^1 \frac{\partial \boldsymbol{\psi}_p}{\partial x} \frac{\partial \boldsymbol{\psi}_q}{\partial x} \, dx, \quad \boldsymbol{\Upsilon}_{mn} = \int_0^1 \frac{d^2 \boldsymbol{\psi}_m}{dx^2} \boldsymbol{\psi}_n \, dx$$

$$\boldsymbol{\eta}_p = \int_0^1 \frac{\partial \boldsymbol{\psi}_p}{\partial x} \frac{dw_x}{dx} dx, \quad \xi_n = \int_0^1 \boldsymbol{\psi}_n \frac{d^2 w_x}{dx^2} dx \tag{34}$$

The first term in (33) is a nonlinear stretching effect, the second corresponds to a linear tension, the third and forth correspond to nonlinear and linear elastic foundation.

In the above, the solution of the general nonlinear displacement equations (21) and (22) was divided into subsolution of a nonlinear ODE with static surface loads (w_x) and solution of nonlinear vibration equation by modal decomposition (w_{xt}) with nonlinear static surface effects (via projections of w_x on $\boldsymbol{\psi}_n$). An approximated analytical solution for $w(x,t)$ can be derived from asymptotic solutions for $w_x(x)$ and $w_{xt}(x,t,\{w_x\})$. For a qualitative investigation, the analysis is restricted to the leading approximation order:

$$w(x,t) = w_{x0}(x) + w_{xt0}(x,t,\{w_{x0}\}) + \mathcal{O}(\varepsilon^1) \tag{35}$$

In the following section, the deflection governing equations (24) and (25), and (26) and (27), are formulated according to the superposition (23) for the particular case of hinged beams. The static approximated solution is extracted by a straight-forward expansion [22] and the dynamic approximated solution is extracted by the method of multiple scales [23], using results from the static solution for the projection terms in (34d,e).

4. Nonlinear vibrations of hinged nano-beams with surface heterogeneity

The case of hinged beams is analyzed here due to the simplified orthogonal relations between its normal modes. Other boundary conditions can be applied similarly.

4.1. General considerations

Consider a hinged beam with a residual static deflection due to a distributed surface residual stresses w_x, subjected to a periodic external excitation $\gamma_2(x,t) = \gamma_2(x)\cos(\Omega t + \phi)$. Following (29)–(34), the solution for w_{xt} is formulated by normal modes expansion with $\boldsymbol{\psi}_n(x) = \sqrt{2}\sin(n\pi x)$ and the following projection terms:

$$\mathbf{K}_{mn} = \boldsymbol{\delta}_{mn} \left[\pi^4 m^4 - \pi^2 m^2 \left(\int_0^1 f_s dx \right) \right] = \boldsymbol{\delta}_{mn} \boldsymbol{\omega}_m^2 \tag{36}$$

$$\boldsymbol{\Gamma}_{pq} = \int_0^1 \frac{\partial \boldsymbol{\psi}_p}{\partial x} \frac{\partial \boldsymbol{\psi}_q}{\partial x} dx = \boldsymbol{\delta}_{pq} \pi^2 pq \tag{37}$$

$$\boldsymbol{\Upsilon}_{mn} = \int_0^1 \frac{d^2 \boldsymbol{\psi}_m}{dx^2} \boldsymbol{\psi}_n dx = -\boldsymbol{\delta}_{mn} \pi^2 m^2 \tag{38}$$

The excitation and coupling vectors ($\mathbf{F}_n(t)$ and $\mathbf{W}_n(x,t)$) are

$$\mathbf{F}_n(t) = \mathbf{k}_n \cos(\Omega t + \phi) \tag{39}$$

$$\mathbf{W}_n(t) = -a \boldsymbol{\varphi}_n(t) \pi^2 n^2 \sum_{p=1}^{\infty} \boldsymbol{\varphi}_p(t) \boldsymbol{\eta}_p - a \frac{1}{2} \pi^2 n^2 \boldsymbol{\varphi}_n(t) \int_0^1 \left(\frac{\partial w_x}{\partial x} \right)^2 dx + a \frac{1}{2} \pi^2 \xi_n \sum_{p=1}^{\infty} \boldsymbol{\varphi}_p^2(t) p^2 + a \xi_n \sum_{p=1}^{\infty} \boldsymbol{\varphi}_p(t) \boldsymbol{\eta}_p \tag{40}$$

$\boldsymbol{\omega}_m$ is the m-th natural frequency, $\mathbf{k}_n$ is the spatial projection of $\gamma_2(x,t)$ over $\boldsymbol{\psi}_n(x)$ and $\boldsymbol{\eta}_n$, ξ_n are the projections of the static deflection $w_x(x)$ over $\boldsymbol{\psi}_n(x)$, as follows:

$$\boldsymbol{\eta}_n = \int_0^1 \frac{\partial \boldsymbol{\psi}_n}{\partial x}\frac{dw_x}{dx}dx = \sqrt{2}\int_0^1 n\pi\cos(n\pi x)\frac{dw_x}{dx}dx \tag{41}$$

$$\xi_n = \int_0^1 \boldsymbol{\psi}_n \frac{d^2w_x}{dx^2}dx = \sqrt{2}\int_0^1 \sin(n\pi x)\frac{d^2w_x}{dx^2}dx \tag{42}$$

Substituting (36)–(42) into (30) yields

$$\frac{\partial^2\boldsymbol{\varphi}_n(t)}{\partial t^2} + \boldsymbol{\omega}_n^2\boldsymbol{\varphi}_n(t) = \varepsilon\begin{bmatrix} \mathbf{k}_n\cos(\Omega t+\phi) - \mu\dfrac{\partial\boldsymbol{\varphi}_n(t)}{\partial t} \\ -a\dfrac{1}{2}\boldsymbol{\varphi}_n(t)\pi^4n^2\sum_{p=1}^{\infty}p^2\boldsymbol{\varphi}_p^2(t) + \mathbf{W}_n(t)\end{bmatrix} \tag{43}$$

Note that due to the hinged boundary conditions, $\boldsymbol{\varphi}_n(t)$ are decoupled from each other and can be found independently.

4.2. Vibration analysis of near resonance excitations

Considering excitations near one of the primary resonances ($\Omega \approx \boldsymbol{\omega}_N$), defined by the detuning parameter $\varepsilon\vartheta$ as

$$\Omega = \boldsymbol{\omega}_N + \varepsilon\vartheta = \sqrt{N^4\pi^4 - N^2\pi^2\left(\int_0^1 f_s\,dx\right)} + \varepsilon\vartheta \tag{44}$$

Following the method of multiple scales [23], the solution of (43) can be approximated by

$$\boldsymbol{\varphi}_n(t,\varepsilon) = \boldsymbol{\varphi}_{n0}(t_0,t_1) + \varepsilon\boldsymbol{\varphi}_{n1}(t_0,t_1) + O(\varepsilon^2) \tag{45}$$

The zero and first approximation orders are extracted from

$$D_0^2\boldsymbol{\varphi}_{n0}(t_0,t_1) + \boldsymbol{\omega}_n^2\boldsymbol{\varphi}_{n0}(t_0,t_1) = 0 \tag{46}$$

$$D_0^2\boldsymbol{\varphi}_{n1}(t_0,t_1) + \boldsymbol{\omega}_n^2\boldsymbol{\varphi}_{n1}(t_0,t_1) = \mathbf{k}_n\cos(\Omega t+\phi) - 2D_0D_1\boldsymbol{\varphi}_{n0}(t_0,t_1) - \mu D_0\boldsymbol{\varphi}_{n0}(t_0,t_1) - a\frac{1}{2}\boldsymbol{\varphi}_{n0}(t)\pi^4n^2\sum_{p=1}^{\infty}p^2\boldsymbol{\varphi}_{p0}^2(t) + \mathbf{W}_n(t)|_{\boldsymbol{\varphi}_{n0}} \tag{47}$$

where $D_i \equiv \partial/\partial t_i$ is a partial derivative operator. Proposing the following solution for the zero approximation order (46):

$$\boldsymbol{\varphi}_{n0}(t_0,t_1) = \tfrac{1}{2}\mathbf{B}_n(t_1)\exp(\mathrm{i}\boldsymbol{\omega}_n t_0) + \mathrm{C.C} \tag{48}$$

Substituting (48) into (47), expanding $\mathbf{W}_n(t)|_{\boldsymbol{\varphi}_{n0}}$, collecting secular terms with $\exp(\mathrm{i}\boldsymbol{\omega}_n t_0)$ and applying the solvability condition, yield for $n=N$

$$\mathrm{i}\boldsymbol{\omega}_N\frac{d\mathbf{B}_N}{dt_1} + \mathbf{B}_1\begin{bmatrix} \dfrac{1}{2}\mu\mathrm{i}\boldsymbol{\omega}_N + a\dfrac{3}{16}\pi^4N^4\mathbf{B}_N\overline{\mathbf{B}}_N \\ +\dfrac{1}{8}a\pi^4N^2\sum_{p\neq N=1}^{\infty}p^2\mathbf{B}_p\overline{\mathbf{B}}_p + \boldsymbol{\mathcal{W}}_N\end{bmatrix} = \frac{1}{2}\mathbf{k}_N\exp(\mathrm{i}(\vartheta t_1+\phi)) \tag{49}$$

and for $n\neq N$

$$\mathrm{i}\boldsymbol{\omega}_n\frac{d\mathbf{B}_n}{dt_1} + \mathbf{B}_n\begin{bmatrix} \dfrac{1}{2}\mu\mathrm{i}\boldsymbol{\omega}_n + a\dfrac{3}{16}\pi^4n^4\mathbf{B}_n\overline{\mathbf{B}}_n \\ +\dfrac{1}{8}a\pi^4n^2\sum_{p\neq N=1}^{\infty}p^2\mathbf{B}_p\overline{\mathbf{B}}_p + \boldsymbol{\mathcal{W}}_N\end{bmatrix} = 0 \tag{50}$$

where $\boldsymbol{\mathcal{W}}_N$ includes secular terms, associated with the nonlinear effect and the static surface induced deflection:

$$\boldsymbol{\mathcal{W}}_N(w_x) = \frac{1}{2}a\left[\frac{1}{2}\pi^2n^2\int_0^1\left(\frac{\partial w_x}{\partial x'}\right)^2dx' - \xi_n\boldsymbol{\eta}_n\right] \tag{51}$$

Note that $\boldsymbol{\mathcal{W}}_N$ is always positive ($\xi_1\boldsymbol{\eta}_1 \le 0$ and $a>0$). If w_x=0, $\boldsymbol{\mathcal{W}}_N = 0$ and (49) and (50) reduce to the familiar form of nonlinear vibrations in pre-stressed beams [19]. Expressing $\mathbf{B}_n$ by

$$\mathbf{B}_n(t_1) = \mathbf{b}_n(t_1)\exp(\mathrm{i}\boldsymbol{\theta}_n(t_1)) \tag{52}$$

where both $\mathbf{b}_n$ and $\boldsymbol{\theta}_n$ are real. Substituting (52) into (49) and (50), dividing into real and imaginary parts and seek for stationary solutions, yields trivial solution for $n\neq N$

$$\mathbf{b}_n|_{ss} = 0, \quad n\neq N \tag{53}$$

and the following amplitude and phase responses for $n=N$:

$$\vartheta_{1,2}=\frac{1}{\omega_N}\left[\frac{3}{16}a\pi^4N^4\mathbf{b}_N^2|_{ss}+\mathcal{W}_N\right]\pm\sqrt{\frac{1}{4\omega_N^2\mathbf{b}_N^2|_{ss}}\mathbf{k}_N^2-\frac{1}{4}\mu^2} \tag{54}$$

$$\theta_N|_{ss}=\phi+\varepsilon\vartheta t-\tan^{-1}\left[\frac{\frac{1}{2}\mu\omega_N}{\frac{3}{16}a\pi^4N^4\mathbf{b}_N^2|_{ss}+\mathcal{W}_N-\omega_N\vartheta}\right] \tag{55}$$

Examining (54) and (55) and recalling that $\mathcal{W}_N\geq 0$, it can be concluded that the static deflection induced by non-uniform surface residual stresses yields positive shifts of the amplitude-response curve (moves to the right) and a decrease of the output phase. Both effects are emphasized as the projection terms ξ_n and η_n increase, where the maximum effect is obtained for $w_x\propto\psi_N(x)$. It can be seen that when $\mathcal{W}_N=0$, (54) and (55) reduce to the standard nonlinear response [19].

To summarize, local changes in the surface properties affect the response of hinged nano-beams in four aspects: (1) changes the resonance frequency via the integrated force component $\int_0^1 f_s\,dx$ (21), (2) changes the residual static deflection (w_x) via both $\int_0^1 f_s\,dx$ and m_s, (3) induce a shift of $\mathcal{W}_N$ in the amplitude-response curve and (4) reduce the output phase shift. The effects of the other beam parameters, γ_2, a and μ, on the beam vibrations are identical to the standard macroscopic analysis and can be found in [19].

4.3. Case study—effect of single surface non-uniformity on the first resonance of hinged nano-beam

Consider a hinged nano-beam with a single surface non-uniformity on its upper surface at $x_a\leq x\leq x_b$, subjected to a singular periodic excitation force at $x=x_\gamma$, as shown in Fig. 3. Denote τ_0 and τ_1 as the surface residual stresses, inside and outside the surface non-uniformity, respectively. Following (14) and (15), the surface residual force and moment are, respectively,

$$f_s(x)=24\frac{1}{Eh}\left(\frac{L}{h}\right)^2\tau_0+12\frac{1}{Eh}\left(\frac{L}{h}\right)^2(\tau_1-\tau_0)R_{x_a,x_b}(x) \tag{56}$$

$$m_s(x)=6\frac{1}{Eh}\left(\frac{L}{h}\right)(\tau_0-\tau_1)R_{x_a,x_b}(x) \tag{57}$$

where $R_{x_i,x_j}(x)$ is the rectangular function

$$R_{x_i,x_j}(x)\equiv\begin{cases}1 & x_i\leq x\leq x_j\\ 0 & \text{else}\end{cases} \tag{58}$$

The zero-order analytical approximation for the static residual deflection function, can be obtained from the straightforward asymptotic expansion [22]. By substituting $w_x=w_{x0}(x)+\mathcal{O}(\varepsilon^1)$ into (24) and (25) and keeping terms with order of ε^0, yields

$$\frac{d^4w_{x0}}{dx^4}+\int_0^1 f_s\,dx\frac{d^2w_{x0}}{dx^2}=\frac{d^2m_s}{dx^2} \tag{59}$$

$$w_{x0}(x=0,1)=0,\quad \frac{d^2}{dx^2}w_{x0}(x=0,1)=m_s \tag{60}$$

Denote G^{hinged} as Green's function for hinged beams

$$G(x,x')=G_1(x,x')R_{0,x'}(x)+G_2(x,x')R_{x',1}(x) \tag{61}$$

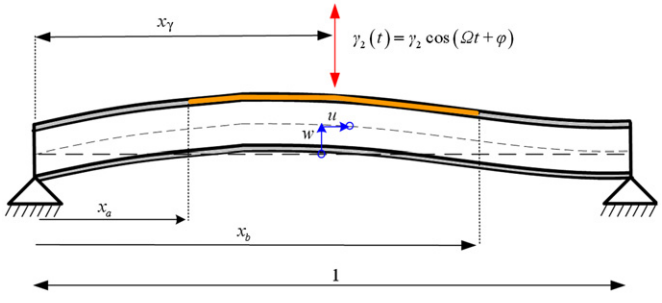

Fig. 3. Hinged nano-beam with surface non-uniformity at $x_a\leq x\leq x_b$ under a singular periodic excitation force $\gamma_2(t)=\gamma_2\cos(\Omega t+\phi)$ at x_γ.

$$G_1(x,x') = G_2(x',x) = \frac{1}{\kappa^3}\left[x\kappa(x'-1) + \frac{1}{\sin(\kappa)}\sin(\kappa x)\sin(\kappa - \kappa x')\right] \tag{62}$$

where $\kappa \equiv \int_0^1 f_s\,dx$. Using Green's identity for self adjoint differential operators in boundary value problems [22], w_{x0} can be extracted from

$$w_{x0}(x) = \int_0^1 G(x,x')\frac{d^2 m_s(x')}{dx'^2}dx' + \left[m_s\frac{dG(x',x)}{dx'}\right]_{x'=0}^{1} \tag{63}$$

Note that since $m_s(x)$ is associated with a rectangular function, (63) is associated with the Dirac operator and its derivatives.

Consider periodic excitations by the singular force at $x = x_\gamma$ near the first resonance frequency:

$$\Omega = \boldsymbol{\omega}_1 + \varepsilon\vartheta = \sqrt{\pi^4 - \pi^2\left(\int_0^1 f_s\,dx\right)} + \varepsilon\vartheta \tag{64}$$

Following (54) and (55), the amplitude-response and phase-response of the vibration function leading order are

$$\vartheta_{1,2} = \frac{1}{\boldsymbol{\omega}_1}\left[\frac{3}{16}a\pi^4\mathbf{b}_1^2|_{ss} + \boldsymbol{\mathcal{W}}_1\right] \pm \sqrt{\frac{1}{4\boldsymbol{\omega}_1^2\mathbf{b}_1^2|_{ss}}\mathbf{k}_1^2 - \frac{1}{4}\mu^2} \tag{65}$$

$$\boldsymbol{\theta}_1|_{ss} = \phi + \varepsilon\vartheta t - \tan^{-1}\left[\frac{\frac{1}{2}\mu\boldsymbol{\omega}_1}{\frac{3}{16}a\pi^4\mathbf{b}_1^2|_{ss} + \boldsymbol{\mathcal{W}}_1 - \boldsymbol{\omega}_1\vartheta}\right] \tag{66}$$

$\mathbf{b}_1$ is the amplitude of the first mode ($\mathbf{b}_{n\geq 2} = 0$) and $\mathbf{k}_1$ is the projection of $\gamma_2(x,t)$ over the first shape mode ($\xi_1(x) = \sqrt{2}\sin(\pi x)$). $\boldsymbol{\mathcal{W}}_1$ includes the effects of the static residual deflection (w_x) through

$$\boldsymbol{\mathcal{W}}_1(w_x) = a\frac{1}{2}\pi^2\int_0^1\left(\frac{\partial w_{x0}}{\partial x}\right)^2 dx - a\boldsymbol{\xi}_1(w_{x0})\boldsymbol{\eta}_1(w_{x0}) + \mathcal{O}(\varepsilon^1) \tag{67}$$

$\boldsymbol{\xi}_1$ and $\boldsymbol{\eta}_1$ are the projection terms of the static deflection on the first vibration mode (see (41) and (42)).

The effect of the surface residual stresses on the beam vibrations was obtained analytically by the perturbation methods and validated by finite elements (FE) simulation. The FE scheme includes a beam composed of Euler–Bernoulli beam elements with fixed axial and vertical displacement constrained in its boundaries. The 300 elements were used to provide highly accurate solution for the beam midpoint deflections, vibrating near its first natural resonance. Surface effects were imposed by an equivalent axial compression force ($\int_0^1 f_s\,dx$) and bending moment distribution $m_s(x)$. Non-zero m_s values were applied along the surface non-uniformity region ($x_a \leq x \leq x_b$). A homogeneous initial conditions were dictated ($w = dw/dt = 0$) and a periodic concentrated force was applied on the x_γ node. The unconditionally stable Newmark "royal road" scheme ($\beta = \gamma = 0.5$ [24]) was used for the time stepping and the beam's midpoints deflections were recorded at the end of each time step. The standard Newton–Raphson method was used for solving the nonlinear system. All iterations

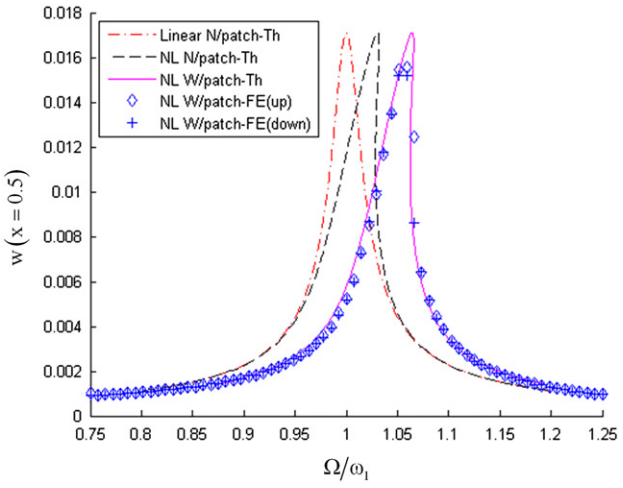

Fig. 4. Amplitude-response for mid-deflections of hinged nano-beam vibrations. Analytical results for the nonlinear beam deflections including surface non-uniformity ("patch") are plotted by the full line. Finite element results with upward and downward detuning are plotted by the diamond and plus symbols, respectively. Theoretical linear and nonlinear responses without surface non-uniformities are plotted for completeness by dashed lines.

exhibited convergence within an accuracy of 10^{-6}. Calculations were stopped when steady-state vibrations were obtained. The output vibration amplitudes were normalized with respect to the static deflection.

Comparison between the approximated analytical solution and results from the FE simulations were conducted via the amplitude-response curve (65). The FE results were recorded for a set of upward and downward detuning parameters, due to an expected jump phenomenon [19]. x_a, x_b and x_γ were arbitrary chosen as 0.25, 0.75, and 0.5, respectively, and the non-scaled parameters were chosen as $\mu = 0.25$, $a = 10^3$, $\int_0^1 f_s\,dx = 1$, $m_s = 0.2$ and $\gamma_2 = 0.2$. The analytical approximation for the amplitude-response curve (nonlinear model with "patch"-surface non-uniformity) was plotted with the corresponding FE simulation results in Fig. 4. Analytical results for the linear and nonlinear cases without surface patch were also plotted for comparison. It can be seen from Fig. 4 that the FE results track closely the analytical predictions, except for the peak region in which the FE exhibit lower maximum value. The discrepancies in the maximum are in the order of 10 percent, which is consistent with the multiple scale approximation. For zero-order perturbation analysis, inaccuracies of $\mathcal{O}(\varepsilon \approx h/L)$ are expected for the amplitude and $\mathcal{O}(\varepsilon^2)$ for the frequency shift. The maximum of the theoretical predictions is greater than the numerical results due to a lack of first-order hardening terms in the analytical approximation, which inherently appear in the FE simulation (followed by (21)). The typical jump phenomenon which is associated with the nonlinear terms is exhibited at $1.06 < \Omega/\boldsymbol{\omega}_1 < 1.07$. It can be seen that the effects of the surface non-uniformity induced a shift of about 3 percent in the amplitude-response curve, which results in a significant amplitude variations for excitations near resonance region. These effects, however, vanish when $|\Omega/\boldsymbol{\omega}_1 - 1| > 20$ percent. The FE results for the amplitude of the higher modes were found to be negligible ($\mathbf{b}_{n\geq 2}|_{ss}/\mathbf{b}_1|_{ss} \approx 0$), which is consistent with the analytical predictions.

5. Applications for novel sensors

The effects of the surface residual stresses on nano-beam vibrations can be used for the design of novel dynamic sensors. Contrary to previous studies which exploited the weaker effect of surface stiffness for adsorption-induced sensing applications with up to 0.5–1 percent differences for micro-scale elements [8,9], in this study we propose to use the dominant surface residual stresses effect to obtain considerable variations.

Consider for example, a hinged beam with uniform surface properties under singular periodic excitation which follows the steady-state amplitude-response curve in Fig. 4 (nonlinear without patch). Assuming surface adsorption of surrounding particles upon the beam's upper surface at $x_a \leq x \leq x_b$. During adsorption, the surface residual stresses are changed, causing a shift in the amplitude-response curve, which changes the vibrations amplitude. By selectively choosing an excitation frequency near the peak of the amplitude-response curve, radical changes are expected for any local change in the surface residual stresses. The effect is especially pronounced in the jump region as demonstrated in Fig. 5, in which the amplitude of the adsorbed beam is three times higher than its non-adsorbed response (results were calibrated relatively to the static deflection). A more detailed response can be seen in Fig. 6, in which both amplitude and phase effects can be appreciated.

For sensing applications, the effects of non-uniform surface residual stresses on the vibrations amplitude should be maximized. Following (54), the resonance shift decreases as the resonance frequencies increase and therefore maximum effect is obtained for the first resonance frequency. The resonance frequency itself can be further decreased by increasing

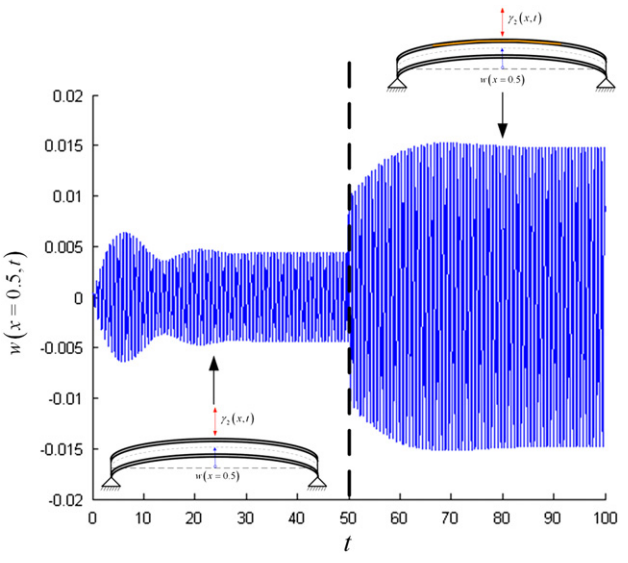

Fig. 5. Effect of surface adsorption on the first mode vibrations of hinged nano-beam, excited by a singular force with $\Omega = 1.05\boldsymbol{\omega}_1$. In t=50, the effect of surface adsorption is induced via changes in $\int_0^1 f_s\,dx$ and m_s. Results for $t > 50$ were calibrated relative to the static deflection.

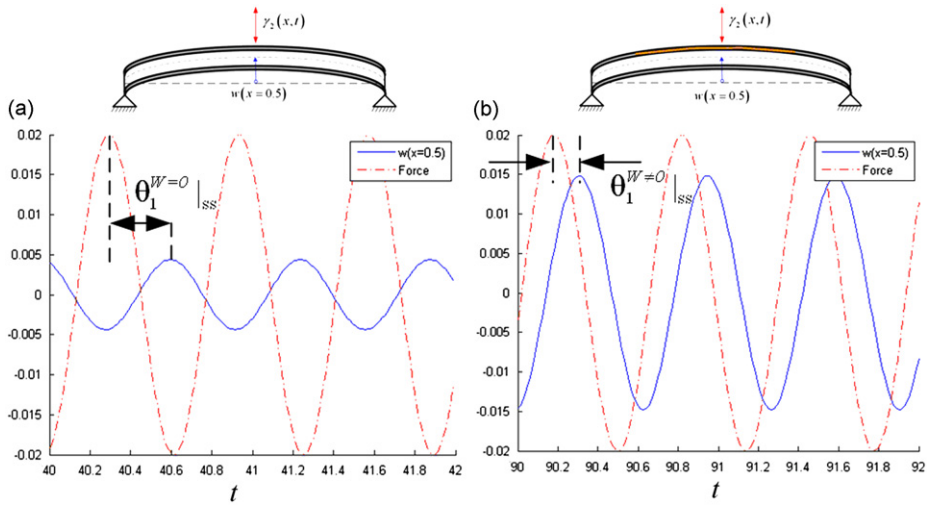

Fig. 6. Zoom on the steady-state vibration regions of the un-adsorbed (a) and adsorbed (b) configurations in Fig. 5, plotted with the external excitation. Both amplitude and phase variations are exhibited.

λ^2 (18) through a stronger compressive surface residual stresses ($\int_0^1 f_s\,dx$) or by dictating axial displacements at the beam edges ($u_0-u_1>0$). Following (51), higher $\mathcal{W}_N$ values are obtained for higher static deflection with larger projection on the normal shape mode. These relations can be optimized by a proper design of the receptor layer for providing maximum stress variations during adsorption and/or by enabling a selective surface adsorption with respect to the desired shape mode.

6. Conclusions

This work analyzed the effect of local surface residual stresses on the resonance frequencies of axially indeterminate nano-beam by including geometrical nonlinearity (mid-plane stretching). A mechanical model was first formulated and separated into two subcases: (1) static deflection including both surface residual force and moment effects and (2) vibrations including the effect of the surface residual force and the static deflection via the nonlinear terms.

The present model unifies and generalizes previous models by considering both nonlinearity and surface heterogeneity. The effects of surface residual stresses on the static deflection and vibrations function were evaluated analytically. A case study of hinged beam was solved by perturbation methods and validated by independent FE simulations. It was found that local changes in the surface residual stresses, cause a considerable effect on the beam vibrations, exhibited by a change of the resonance frequency and a shift in the amplitude-response curve.

In cantilevers, the commonly used dynamic sensing mechanisms, surface residual stresses have a negligible effect and sensing is conducted via adsorption-induced changes in surface modulus. Since the surface modulus effect is much weaker than the surface residual stresses, such detecting mechanisms usually exhibit poor sensitivity and are therefore less attractive than equivalent static sensors. In this work, we enabled to couple between the surface residual stresses and the nano-beams vibrations. Local changes in the surface residual stresses exhibited amplitude variations of about 5–10 times greater than in corresponding cantilever configuration. The sensitivity of such nano-beam-based sensors can be further optimized by a proper design of the surface heterogeneity. In addition, since the static deflection was evaluated separately and a priori to the vibrations amplitude, it can be used as an additional sensing parameter for improving detecting capabilities.

Although this work is oriented for nano-scale beams with surface heterogeneity, the analysis can be applied on macroscopic beams with residual deflections.

References

[1] R.E. Miller, V.B. Shenoy, Size-dependent elastic properties of nanosized structural elements, *Nanotechnology* 11 (2000) 139–147.
[2] M.E. Gurtin, A. Ian Murdoch, A continuum theory of elastic material surfaces, *Archive for Rational Mechanics and Analysis* 57 (4) (1975) 291–323.
[3] C.W. Lim, L.H. He, Size-dependent nonlinear response of thin elastic films with nano-scale thickness, *International Journal of Mechanical Sciences* 46 (11) (2004) 1715–1726.
[4] P. Lu, L.H. He, H.P. Lee, C. Lu, Thin plate theory including surface effects, *International Journal of Solids and Structures* 43 (16) (2006) 4631–4647.
[5] H. Sheng, et al., Free vibration analysis for micro-structures used in MEMS considering surface effects, *Journal of Sound and Vibrations* 329 (2) (2010) 236–246.
[6] B. Bar On, E. Altus, E.B. Tadmor, Surface effects in non-uniform nanobeams: continuum vs. atomistic modeling, *International Journal of Solids and Structures* 47 (9) (2010) 1243–1252.
[7] J.N. Reddy, *Mechanics of Laminated Composite Plates and Shells: Theory and Analysis*, CRC, 2004.

[8] P. Lu, H.P. Lee, C. Lu, S.J. O'Shea, Surface stress effects on the resonance properties of cantilever sensors, *Physical Review B* 72 (8) (2005) 85405.
[9] J. Tamayo, D. Ramos, J. Mertens, M. Calleja, Effect of the adsorbate stiffness on the resonance response of microcantilever sensors, *Applied Physics Letters* 89 (2006) 224104.
[10] J.Q. Zhang, S.W. Yu, X.Q. Feng, G.F. Wang, Theoretical analysis of adsorption-induced microcantilever bending, *Journal of Applied Physics* 103 (2008) 093506.
[11] M.J. Lachut, J.E. Sader, Effect of surface stress on the stiffness of cantilever plates, *Physical Review Letters* 99 (20) (2007) 206102.
[12] M.E. Gurtin, X. Markenscoff, R.N. Thurston, Effect of surface stress on the natural frequency of thin crystals, *Applied Physics Letters* 29 (1976) 529.
[13] R. Berger, E. Delamarche, H.P. Lang, C. Gerber, J.K. Gimzewski, E. Meyer, H.J. Guntherodt, Surface stress in the self-assembly of alkanethiols on gold, *Science* 276 (5321) (1997) 2021.
[14] H.P. Lang, M.K. Baller, R. Berger, C. Gerber, J.K. Gimzewski, F.M. Battiston, P. Fornaro, J.P. Ramseyer, E. Meyer, H.J. Guntherodt, An artificial nose based on a micromechanical cantilever array, *Analytica Chimica Acta* 393 (1–3) (1999) 59–65.
[15] M. Alvarez, A. Calle, J. Tamayo, L.M. Lechuga, A. Abad, A. Montoya, Development of nanomechanical biosensors for detection of the pesticide DDT, *Biosensors and Bioelectronics* 18 (5–6) (2003) 649–653.
[16] K.M. Hansen, T. Thundat, Microcantilever biosensors, *Methods* 37 (1) (2005) 57–64.
[17] B. Bar On, E. Altus, Stochastic surface effects in nanobeam sensors, *Probabilistic Engineering Mechanics* 25 (2) (2009) 228–234.
[18] S. Cherian, T. Thundat, Determination of adsorption-induced variation in the spring constant of a microcantilever, *Applied Physics Letters* 80 (2002) 2219.
[19] A.H. Nayfeh, D.T. Mook, *Nonlinear Oscillations*, Wiley-VCH, 1995.
[20] W. Haiss, Surface stress of clean and adsorbate-covered solids, *Reports on Progress in Physics* 64 (2001) 591–648.
[21] B. Bar On, Surface Effects on the Mechanical Properties of Heterogeneous Nano-beams, PhD Thesis, Technion, Israel Institute of Technology, 2010.
[22] C.M. Bender, S.A. Orszag, *Advanced Mathematical Methods for Scientists and Engineers: Asymptotic Methods and Perturbation Theory*, Springer-Verlag, 1999.
[23] A.H. Nayfeh, *Perturbation Methods*, Wiley, New York, 1973.
[24] J.N. Reddy, *An Introduction to Nonlinear Finite Element Analysis*, Oxford University Press, USA, 2004.